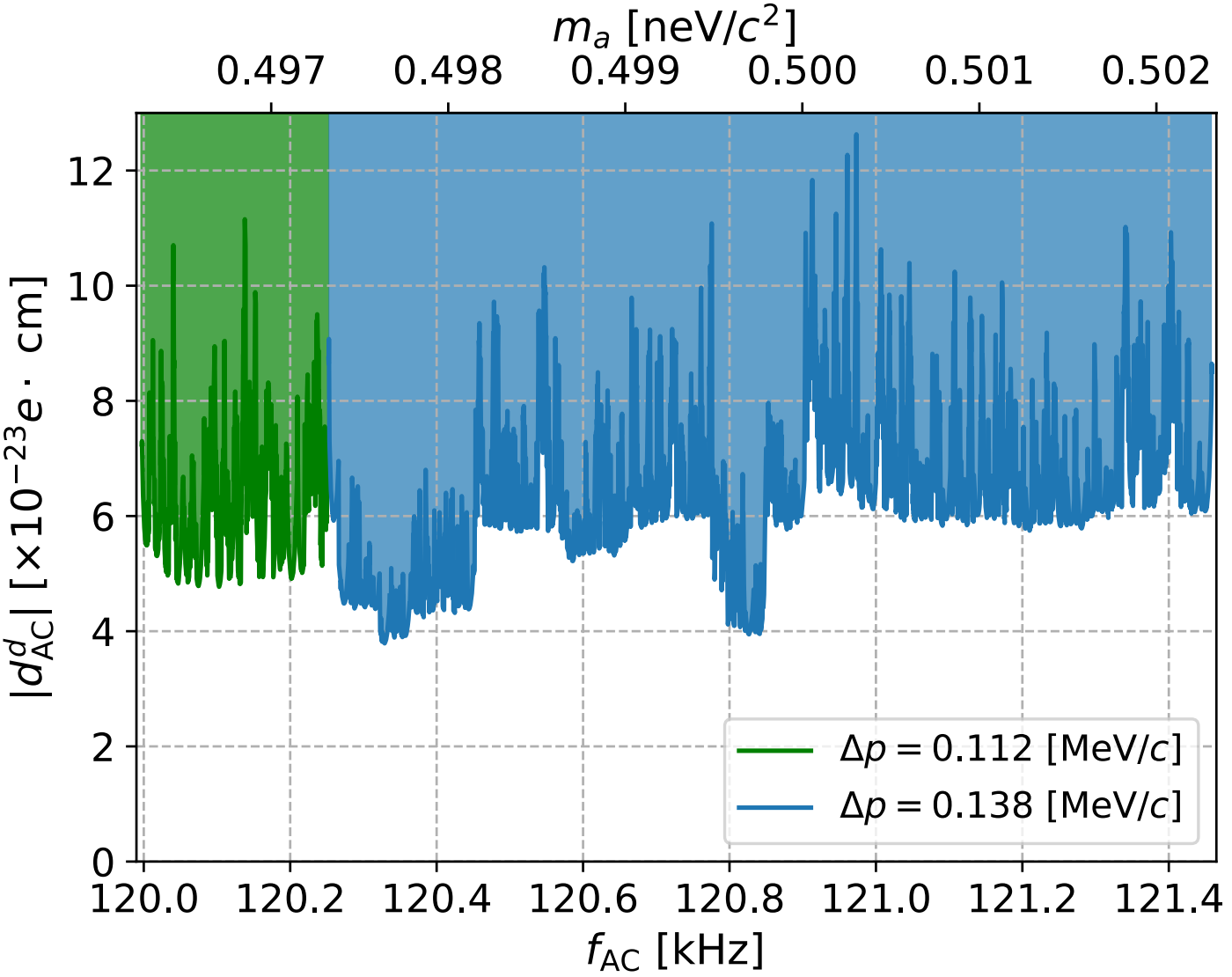

Annual Report 2022

Institut für Kernphysik · COSY

Jül-4435

Annual Report 2022

Institut für Kernphysik / COSY

DIRECTORS AT THE IKP

Experimental Hadron Structure (IKP-1, IKP-2):	**Prof. James Ritman**
Theory of the Strong Interactions (IKP-3/IAS-4):	**Prof. Ulf-G. Meißner**
Large-Scale Nuclear Physics Equipment (IKP-4):	**Dr. Ralf Gebel (managing director)**

EDITORIAL BOARD

Dr. Christian Böhme
Dr. Ralf Gebel
Prof. Frank Goldenbaum
Dr. Dieter Grzonka
Prof. Christoph Hanhart
Dr. Volker Hejny
Dr. Andro Kacharava
Dr. Vsevolod Kamerdzhiev
Prof. Andreas Lehrach
Prof. Livia Ludhova
Prof. Thomas Luu
Prof. Ulf-G. Meißner
Prof. James Ritman
Susan Schadmand, Ph.D. habil.
Dr. Thomas Sefzick

Cover picture: The cover picture shows the sensitivity at a 90% confidence level for excluding oscillating electric dipole moments (EDMs) of the deuteron induced by axion-like particles as measured by the JEDI collaboration. The frequency range shown is $120-121{:}4\,\mathrm{kHz}$, corresponding to an axion mass range of $0{:}495-0{:}502\,\mathrm{neV}/c^2$. The exclusion region is represented by the lighter filled areas, while the darker lines indicate the upper limit of the oscillating EDM. The green and blue colors are used to distinguish between two experimental settings, with the green and blue areas representing measurements with a momentum change per cycle of $\Delta p = 0{:}112\,\mathrm{MeV}/c$ and $\Delta p = 0{:}138\,\mathrm{MeV}/c$, respectively. More detailed information can be found in Sect. 2.1.

Contents

Preface vi

1 Experimental Activities for FAIR 1
- 1.1 X reconstruction with realistic track nders for PANDA . . . 1
- 1.2 Beamtime (Phase-0) at HADES . . . 2
- 1.3 KOALA Experiment . . . 3

2 Storage Ring Based EDM Search 3
- 2.1 Axion Searches . . . 4
- 2.2 Electric Dipole Moment (EDM) Searches . . . 5
- 2.3 Proof of Principle of the Pilot Bunch Technique . . . 6
- 2.4 Investigation of Proton Spin Coherence Time . . . 7
- 2.5 Beam and Spin Tracking . . . 8
- 2.6 Design Study of a Dedicated EDM Ring . . . 9
- 2.7 Outlook: Experiments with Polarized Beams and Targets at the GSI/FAIR Storage Rings . . . 10

3 Neutrino Physics 10
- 3.1 Borexino latest results with solar neutrinos . . . 10
- 3.2 Towards completion of the JUNO detector . . . 13
- 3.3 Online Scintillator Internal Radioactivity Investigation System (OSIRIS) of JUNO . . . 15

4 Accelerator Research 16
- 4.1 Developments at COSY . . . 16
- 4.2 Progress of the HESR . . . 18

5 Further Activities 20
- 5.1 LHCb Polarized Target Experiment . . . 20
- 5.2 A new Method to polarize Atoms, Molecules and their Ions . . . 21

6 Theoretical Investigations 23
- 6.1 Introduction . . . 23
- 6.2 Emergent geometry and duality in the carbon nucleus . . . 23
- 6.3 Hyperon-nucleon interaction in chiral EFT . . . 24
- 6.4 Charge-symmetry breaking in $A = 7$ and $A = 8$ hypernuclei . . . 25
- 6.5 Prediction of ve- avoured penta-quarks . . . 26
- 6.6 Do near-threshold molecular states mix with neighbouring $\bar{Q}Q$ states? . . . 26
- 6.7 Localization of electron wavefunctions in hybrid nanoribbons . . . 27
- 6.8 Criticality in brain dynamics . . . 28

A Beam Time at COSY in 2022 29

B Committees 31
- B.1 CBAC – COSY Beam Time Advisory Committee . . . 31
- B.2 Committee Service . . . 31

C Publications 33
- C.1 Journal Articles . . . 33

D Talks, Colloquia and Proceedings 39
- D.1 Conference and Workshop Contributions . . . 39
- D.2 Colloquia . . . 45

E Academic Degrees 47
- E.1 Dissertation / PhD Theses . . . 47
- E.2 Master Theses . . . 48
- E.3 Bachelor Theses . . . 48

F Awards 49

G Third Party Funded Projects 50

H Collaborations 51

I Conferences and Outreach Activities (Co-)Organized by the IKP 52
I.1 PSTP2022 Workshop 52
I.2 Georgian-German Science Bridge: 9th GGSWBS Workshop in Tbilisi and Kutaisi: Health as a Global Challenge: contributions by GGSB and its SMART|Labs" 52
I.3 Particle physics academy and training program for high school students 2022 53
I.4 Eighth Annual Meeting of the Programme "Matter and Technologies" 53
I.5 HESR Get Together Workshops 54

J Teaching Positions 55

K Personnel 56

L Individual Contributions 59
Accelerator Research 61
Experimental Activities for FAIR 77
Further Activities 90
Storage Ring Based EDM Search 97
Neutrino Physics 112

Preface

This Annual Report 2022 compiles the joint activities of the Institute for Nuclear Physics (IKP) of the FZ-Jülich (FZJ) and the departments FAIR Research at NRW (FFN) and HESR of GSI-FAIR together with international collaborations at COSY as well as experiments of our scientists at other laboratories. This has been the second year of the incremental transfer of most of the activities at IKP and the corresponding resources from FZJ to GSI, a process called TransFAIR. Two new departments have been established at GSI. The experimental activities at IKP-1 and IKP-2 and part of the infrastructure activities are transferred into the department FFN (FAIR-Forschung-NRW). The accelerator-related and the remaining infrastructure activities are transferred to the department HESR and other organizational units at FAIR. Despite these organizational changes, the following experimental, theoretical and accelerator highlights have been achieved:

The contributions of FFN and the IKP theory feature prominently in the newly approved network of experimental and theoretical groups within NRW (Bochum, Bonn, Jülich, Münster, Wuppertal and GSI-Darmstadt as associated partner). The network is called NRW-FAIR and has over 16 MEUR available for the upcoming four years, and also provides a basis to establish of a signi cant part of FFN at universities in NRW.

A four week beam time was successfully performed as part of FAIR Phase0 to study the production and decay of excited hyperons with two new $\bar{P}$ANDA-type Straw Stations, in the upgraded HADES spectrometer. The new detectors operated stably without failures and the electronic readout of the straw signals were constant with low noise levels up to the highest particle rates of a few $\times 10^5$ s^{-1} per straw.

The KOALA experiment was designed and built to precisely measure the total and elastic cross section of antiproton-proton elastic scattering. In commissioning experiments at COSY, it was learned that the results depend signi cantly on the beam alignment and the vacuum in the scattering chamber, which is now being studied in further detail with simulations.

The performance of $\Lambda\Lambda$ reconstruction with realistic track nders for PANDA has been substantially improved. Hyperon reconstruction requires a high track nding ef ciency for both primary tracks and secondary tracks, i.e. originating from a displaced secondary vertex. The new track nders improve the full event reconstruction rate for hyperons by as factor four.

The JEDI- and CPEDM collaborations continued towards their goal to provide a scienti c infrastructure for the search for charged-particle electric dipole moments. In September 2022 the Advanced Grant "Search for electric dipole moments using storage rings" (srEDM, #694340) of the European Research Council was successfully concluded. A design study of the prototype storage ring is envisaged as the next step.

In 2019 the JEDI Collaboration explored a new method to search for axions or axion-like particles (ALPs) in storage rings using an in-plane polarized deuteron beam. The experiment entailed a scan of the spin precession frequency. In 2022 the data analysis was nished, and a corresponding publication was submitted. No ALP resonance was observed and upper limits of the oscillating EDM component of the deuteron and the corresponding axion coupling constants are provided.

The main goal of the JEDI precursor experiment is to make the rst direct measurement of the deuteron EDM. This includes performing experiments on prolonging and understanding the spin coherence time (SCT) of cooled and bunched deuterons at a beam momentum of $p = 970$ MeV/c. It has been shown that sextupole con gurations leading to small chromaticities in the horizontal and vertical plane result in long SCTs in the order of $\tau = 1000$ s. A rst run on proton SCT was performed at the beginning of 2022. Detailed beam and spin dynamics simulations have been performed to explain experimental results with polarized deuterons and protons at COSY and determine the optimal setting for polarized protons.

Together with the INFN Section of Ferrara, IKP has developed storage cells for gaseous targets, with signi cant impact in the eld of experimental hadronic physics. This competence is being made available to LHCspin, which aims at installing a polarized gas target to bring spin physics at LHC for the rst time. With strong interest and support from the international theoretical community, LHCspin offers unique opportunities by complementing both existing facilities and the future Electron-Ion Collider.

A Letter of Intent entitled "Towards experiments with polarized beams and targets at the GSI/FAIR storage rings" has been submitted to the GPAC. The committee encouraged the authors to submit a full proposal. Among the physics topics proposed are axion/ALP searches and the measurement of parity even time-reversal odd analyzing power in polarized proton tensor polarized deuteron scattering.

Together with the Borexino collaboration, the IKP neutrino group published the first precise measurement of the Earth's orbital parameters based solely on solar neutrinos. In 2022, the first measurement of sub-MeV solar neutrinos using their associated subdominant Cherenkov radiation was presented by Borexino. To investigate neutrinos from Fast Radio Bursts (FRBs) a search for an excess in the number of events produced by neutrino-electron elastic scattering and the inverse beta-decay on protons (IBD) has been performed using the full exposure Borexino data set. No statistically significant increase in the number of events over the backgrounds was observed. Furthermore, the strongest upper limits on FRB-associated neutrino fluences of all flavors is obtained in the 0.5 to 50 MeV neutrino energy range. JUNO will be the first multi-kton Liquid Scintillator (LS) detector currently under construction in Jiangmen, China. The success of JUNO strongly depends on the levels of radiopurity that will be achieved. The achieved level of LS radiopurity will be tested in 20 ton detector of OSIRIS (Online Scintillator Internal Radioactivity Investigation System). Within OSIRIS, the neutrino group is responsible for the source insertion calibration system, a refurbished Automated Calibration Unit.

The IKP theory group studies the strong interactions in their various settings, spanning topics in hadron structure and dynamics, the nuclear many-body problem, symmetry tests in Quantum Chromodynamics (QCD), physics beyond the Standard Model, strongly correlated electronic systems and brain dynamics. The first focus of the theory group is the formulation and application of effective field theories for precision hadron and nuclear physics based on the symmetries of QCD. The second focus is related to high-performance computing in nuclear, hadronic and condensed matter physics, spear-headed by the work on nuclear lattice simulations. This year, we added machine-learning techniques to our toolbox.

Since July 2012, the group is heavily involved in the activities of the collaborative research center “Symmetries and the emergence of structure in QCD” (CRC 110) together with researchers from Bonn University, TU München, Ruhr-Universität Bochum, IHEP/CAS (Beijing, China), ITP/CAS (Beijing, China) and Peking University (China). This CRC is presently in its third and final funding period. A further strengthening of the group was achieved through the ERC Advanced Grant “EXOTIC” that began in November 2021. It focuses on precision calculations in nuclear and hypernuclear physics on the lattice and exploring fine-tunings in nuclear reactions and the role of anthropic considerations. Since this year, the IKP theory group is also involved in the NRW-FAIR network funded by the Ministry of culture and science of the state of Northrhine-Westfalia. Some of the highlights of all of these activities are discussed in this report.

One central element unifying IKP is the operation of and experiments with COSY. A second element is the realization of the High Energy Storage Ring (HESR) for the PANDA experiment. The completion of all accelerator components is coming to an end and all major systems are ready to be stored until installation starts for the completion of FAIR. All 46 bending dipole magnets have been equipped with the necessary vacuum chambers and delivered to the storage in Weiterstadt. This includes four magnets that were prepared for the SPARC experiment and therefore possess modified vacuum chambers, where a laser beam for the experiment can be passed in and out. One of the cavities for the HESR was installed in COSY for testing already in late 2021. In early 2022 some initial tests including the recording of calibration data were performed. Since then it has been used to accelerate the beam during the operation of COSY. As expected its stability and reliability could be demonstrated.

Researchers from JCNS at FZJ have achieved a breakthrough by delivering the first neutrons with a new powerful target/moderator technology developed in Jülich. Currently, the platform houses three beamlines: a detector test stand, a time-of-flight (ToF) diffractometer, and the HERMES neutron reflectometer from the decommissioned Orphée reactor, which was contributed through a collaboration with LLB (Saclay). Both thermal and cold neutrons were measured at all three positions around the TMR facility.

The success of our institute is built on the efforts of all its members, and with this report, we can share our achievements. We are pleased to express our sincere gratitude to everyone in the institute for their efforts during this challenging year. The achievements presented in this report would not have been possible without the dedication of our technicians and engineers, the service groups, our colleagues in the FZJ infrastructure, and the students who advanced the scientific work. We continued in COVID conditions followed by the effects of the Russian invasion of Ukraine. There were impressive results and progress across many activities. We thank all for their continued commitment and sense of responsibility, which enabled the institute to perform excellently this year despite highly challenging circumstances.

Jülich, March 2023

Ralf Gebel, Ulf-G. Meißner, Jim Ritman

1 Experimental Activities for FAIR

1.1 X reconstruction with realistic track finders for PANDA

Hyperon reconstruction requires a high track finding efficiency not only for primary tracks but also for secondary tracks originating from a displaced secondary vertex. The reason is that hyperons have a long lifetime and often decay into Λ particles, which also have a long lifetime with a mean decay length of a few cm. Secondary track finding is a more computationally intensive task than primary track finding, where the interaction point (IP) can be used to simplify the calculation and to reduce the number of parameters. Therefore a combination of primary and secondary track finders leads to the best performance in terms of efficiency and computing time. In this work the combination of primary and secondary track finders were investigated by analyzing a benchmark hyperon reaction chain for PANDA: $p\bar{p} \to X(1820)\,\bar{X}^{+} \to \Lambda K^{-}\bar{\Lambda}p^{+} \to pp\,K^{-}p^{+}\bar{p}p^{+}$. The reaction chain contains one primary particle (K^{-}) and five secondary particles (p, π^{-}, p^{+}, $\bar{p}$, p^{+}). An example event display is shown in Fig. 1. Two different primary track finders were combined with a newly developed secondary tracker. The two investigated primary track finders are the currently used track finder in PANDA, which is called the standard tracker, and a newly developed track finder based on Hough transformations. The efficiencies are here always defined as the fraction of found tracks divided by the number of reconstructable tracks. A track is defined as reconstructable if it has at least four hits in the MVD or six hits in all tracking detectors (MVD, STT, GEM).

Figure 1: An example event of the $p\bar{p} \to X(1820)\,\bar{X}^{+}$ reaction. The ideal tracks are shown in green, the tracks found by the combination of Hough and Secondary track finder are shown in red.

Comparing only the primary track finders for tracks in the target spectrometer shows that the standard tracker has a higher efficiency for the primary particle (Standard: 88.2 %, Hough: 82.4 %). However, the efficiency of the secondary particles is higher for the Hough track finder (table 1). The full event reconstruction rate for the Hough track finder is 5.9 %, which is more than twice that of the standard tracker with only 2.4 %. This is a consequence of the higher efficiencies for secondary tracks for the Hough track finder.

The combination of primary and secondary track finders (table 2) improves the reconstruction rate in the target spectrometer of the secondary tracks (Standard + Secondary: 56.0 % - 73.6 %, Hough + Secondary: 58.8 % - 78.3 %). Here the improvement of the standard tracker is larger than the improvement of the Hough track finder, since the Hough track finder itself had already a better efficiency. In both cases the secondary track finder improves the full event reconstruction rate. For the standard track finder an improvement by a factor of four could be reached (from 2.4 % to 9.9 %). The increase in efficiency for the Hough and secondary track finder is less pronounced with an improvement of about 40 % (from 5.9 % to 8.2 %). The reason for the slightly lower efficiency of the combination of Hough and secondary track finder compared to the combination of standard and secondary track finder is that the Hough tack finder itself has a much better reconstruction rate for secondary tracks. However, the momentum resolution of these tracks is poorer. Consequently, the Hough track finder finds secondary tracks with a poor momentum resolution which then are not available for the secondary track finder anymore. Here, optimizing the Hough track finder to only find primary tracks promises a stronger improvement for the combination with the secondary track finder. The new track finders (Hough and Secondary track finder) both lead to an improvement of the full event reconstruction rate of the investigated hyperon decay. The full event reconstruction rate, which also takes the detector acceptance into account, could be improved by a factor of four to a reconstruction efficiency of 1.2 % for the combination of the standard and secondary track finders, compared to 0.3 % for the full event reconstruction rate reached with only the standard tracker.

	Standard	Hough
K^{-}	88.2	82.4
π^{-}	61.6	62.3
p	43.2	62.8
p^{+} (X+)	52.5	69.2
$\bar{p}$	50.9	51.9
p^{+}	32.3	51.6
Full event	2.4	5.9

Table 1: Reconstruction efficiencies of the final state particles found in the target spectrometer and reconstruction efficiency of the full event using only the primary track finder.

Currently, both the Hough and the Secondary track finders reconstruct only the x-y-component of a particle track. The z-component is reconstruction using Monte Carlo information from the simulated tracks. The next step towards a realistic track finding in the target spectrometer is to combine the algorithms with a realistic p_t finder, which already exists in PANDA. Additionally, an online capability of the Hough track finder has already been tested by porting the algorithm to a GPU. A speed-up factor of four could be achieved with a medium size GPU. Of particular interest is also the investigation of the online capability of the Secondary track finder.

	Standard + Secondary	Hough + Secondary
K	88.8	86.5
P	71.5	70.4
p	65.7	73.5
p^+ (X+)	73.6	78.3
$\bar{P}$	56.5	58.6
p^+	56.0	63.5
Full event	9.9	8.2

Table 2: Reconstruction efficiencies of the final state particles found in the target spectrometer and reconstruction efficiency of the full event using primary and secondary track finders.

1.2 Beamtime (Phase-0) at HADES

As part of the FAIR phase-0 program, a beam time of four weeks was successfully performed in spring 2022 to study the production and decay of excited hyperons with two new, $\bar{P}$ANDA-type Straw Stations (STS1 and STS2) in the upgraded HADES spectrometer. The proton beam with kinetic energy of 4.5 GeV was focused on a liquid hydrogen target. In addition to the new STS tracking stations, there was a new RPC detector for time-of-flight measurements covering the polar-angle range from about 0.7^o up to 6.5^o to complement the forward going tracks in the STS. A stable operation of the STS detectors without any failures and stable electronic readout of the straw signals with constant, low noise levels up to the highest particle rates of a few $10^5 s^{-1}$ per straw was achieved. This result verifies the various quality assurance methods and measurements during the preparation and set up of the systems, which will be adopted for the $\bar{P}$ANDA-STT.

The calibration methods of both STS stations were developed and the calibration of the space – drifttime relation for each of the 1728 single straws in the STS has been completed for the beam time data. Fig. 2 shows as an example the result of the parametrized isochrones radius - drifttime relation r(t) (red line) and the comparison with a simulation of ionizing proton tracks through a single straw (green line: fit of the track distance versus drifttime points). As expected, close to the wire the measurement of small track distances is distorted by the varying and Poisson-distributed distances of the ionization clusters along the track path, which limits the resolution in this region. Above a track-to-wire distance of about 0.6 mm the agreement between the simulated drift motion and r(t) calibration of the data is very good.

Figure 2: Drift time simulation (Garfield) of proton tracks passing through a single straw and r(t) parametrization (green line: fit to the simulation, red line: r(t) calibration for the in-beam data)

Part of the calibration is the determination of the maximum drift time of a straw, which contains all smearing effects of the drifttime measurement and systematic errors, from the straw geometry, drift gas, electric field, electronic readout up to the drifttime extraction and calibration with a parametrization of the isochrone radius - drifttime relation r(t). Fig. 3 shows the distribution of the maximum drifttime for all 704 straws in the STS1 with a mean value of 164 ns. The obtained very low spread of 3.2 ns (σ) of the distribution corresponds to very low differences in the maximum isochrone radius for all straws of less than 40 µm, which is less than 0.8% of the pressurized straw tube inner radius of 5.05 mm. The result confirms the precise geometry of the $\bar{P}$ANDA-type straw technology with self-supporting, pressurized and thin-wall film tubes.

Note, that a few straw channels in the region 150 to 155 ns in Fig. 3 have a low number of entries in the drifttime spectrum, where the determination of the start and end of the spectrum yields slightly lower values for the maximum drifttime.

Proton-proton elastic scattering events are used to determine the integrated luminosity for the production run. Events were selected that contain one proton in the STS tracking stations with a polar angle (θ) in the region of $3 < q_{STS} < 6$ in coincidence with a proton in the polar angular range $70 < q_H < 79$ measured by the main HADES spectrometer. Kinematic contraints are used to

Figure 3: Distribution of the maximum drifttime (ns) for all straws in the STS1. A gaussian fit (red line) to the data obtained a mean value of 164 ns and width of 3.2 ns (σ).

suppress the background in the data sample. The cross-section of proton-proton elastic scattering into this angular range is σ_{el}=4.4$^{+0.8}_{0.3}$ mb as obtained by interpolation between measurements from other experiments. The reconstruction efficiency is determined by a comparison with proton-proton elastic events from simulation. The preliminary time integrated luminosity for the four week beamtime is 5.6 0.4 pb^{-1} and will allow studies of e.g. hyperon production and decay channels and the experimentally unexplored process of hyperon Dalitz decays. More details about the proton-proton elastic scattering analysis and determination of the integrated luminosity are discussed in this annual report as a separate individual report by G. Perez-Andrade (see page 85).

1.3 KOALA Experiment

The KOALA experiment was designed and built to measure the antiproton-proton elastic scattering in order to gain precise knowledge of the total cross section as well as the elastic cross section. The main idea of KOALA is to measure the region covering the Coulomb-nuclear interference, in which Coulomb scattering can be used for an absolute normalization of the luminosity. KOALA consists of a hydrogen cluster-jet target, a recoil detector and a forward detector to obtain a wide range of squared four-momentum transfer, i.e., $|t|$=0.0008-0.1 (GeV/c)^2. The recoil detector comprises four semiconductor strip energy sensors measuring the kinetic energy and emitting angle of the recoil protons. Four pairs of plastic scintillator bars as the forward detector are located symmetrically at the vertical and horizontal direction close to the beam axis. With the commissioning experiments at COSY, it was learned that the precision of the measurement is significantly impacted by the finite beam misalignment as well as the poor vacuum in the scattering chamber.

Figure 4: Schematic layout of the KoalaSoft framework.

To pursue an even higher precision of the measurements, the current focus of KOALA is to investigate such constraints by software studies. Based upon FairRoot, which combines the VMC library and the ROOT package, the KoalaSoft framework has been developed for both data analysis and simulation study. As illustrated in Fig. 4, the KoalaSoft package has been devised to be modularized concerning a sustainable development and maintenance. In order to implement the same analysis codes either for simulated data or for experiment data, special attention has been paid for the data format. The unpacked experiment data as well as the simulated data after digitization can be further processed with the same analysis routines. Benefiting from the modularization, new features or developments can be readily added to the framework.

To enable investigations of the impact of the beam and target on the overall precision of the experiment, a preliminary simulation chain for proton-proton elastic scattering has been implemented. It can be used to generate proton-proton elastic events and reconstruct the t-distribution for further studies. The new features to simulate the the beam misalignment and the beam halo or generate background from a poor vacuum from the hydrogen cluster target are being implemented.

2 Storage Ring Based EDM Search

The JEDI- and CPEDM-collaborations continued investigations and measurements towards their goal to provide a scientific infrastructure which enables the search for charged-particle electric dipole moments with unprecedented sensitivity. At the end of September 2022, a major milestone was reached with the successful conclusion of the Advanced Grant „Search for electric dipole moments using storage rings“ (srEDM, #694340) of the European Research Council with Principal Investigator Hans Ströher and additional beneficiaries University of Ferrara (Paolo Lenisa) and RWTH Aachen University

Preliminary

Preliminary

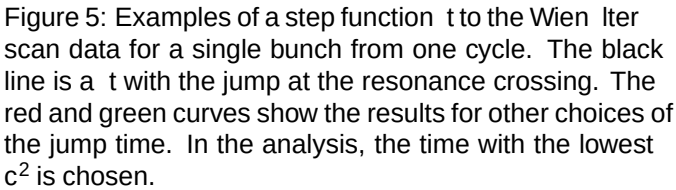

Figure 5: Examples of a step function fit to the Wien filter scan data for a single bunch from one cycle. The black line is a fit with the jump at the resonance crossing. The red and green curves show the results for other choices of the jump time. In the analysis, the time with the lowest χ^2 is chosen.

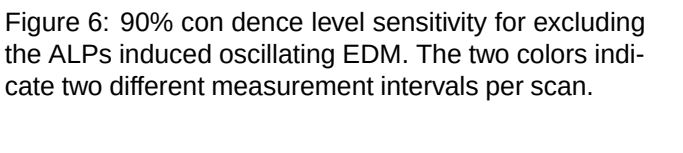

Figure 6: 90% confidence level sensitivity for excluding the ALPs induced oscillating EDM. The two colors indicate two different measurement intervals per scan.

(Jörg Pretz). As the next step, the collaborations envisage a design study of the prototype storage ring.

2.1 Axion Searches

In 2019 the JEDI Collaboration performed a first measurement at COSY exploring a new method to search for axions or axion-like particles (ALPs) in storage rings by using an in-plane polarized deuteron beam. The experiment scanned momenta near 970 MeV/c and entailed a scan of the spin precession frequency. At resonance between the spin precession frequency of deuterons and the ALP-induced EDM oscillation frequency, there should be an accumulation of the polarization component out of the ring plane. The beam momentum and, consequently, the spin precession frequency were ramped to search for a vertical polarization change. During 2022 the data analysis has been finished, and a corresponding publication has been submitted[1]. No ALP resonance was observed and upper limits of the oscillating EDM component of the deuteron and the corresponding axion coupling constants are provided.

The pseudoscalar nature of axions and ALPs allows interactions of the oscillating axion/ALP field $a(t)$ with the spin of nucleons and nuclei by two different mechanisms: coupling to the electric dipole moment of a non-self-conjugate particle with non-zero spin or by the gradient of the field, known as the axion-wind effect. The first coupling leads to an oscillating component d_{AC} of the particle's total EDM pointing parallel to the spin direction. The second coupling, the axion wind, causes the spin of a nucleon or nucleus to rotate about the gradient of the axion field, which is analogous to a magnetic field parallel to the particle momentum. Both effects cause resonant rotation of the spin when the precession frequency of the spin matches the oscillation frequency of the axion field, resulting in a build-up of vertical polarization. The measurement principle is similar to a Froissart-Stora scan, in which the axion field is treated as an RF spin resonator scanning the spin precession frequency using a slow momentum ramp. In this way, most of the systematic effects that occur in a static EDM measurement are not present here.

During the experiment, a total of 103 partially overlapping frequency intervals were scanned, covering a range from 119.997 kHz to 121.457 kHz or an axion mass range of 4.95–5.02 neV/c^2. For each scan, the phase of the oscillating electric dipole moment relative to the in-plane precession motion is unknown. This could cause a ALP to be missed during a single scan, since the magnitude of the out-of-plane rotation is affected by this relative phase. To avoid this, four beam bunches were used simultaneously so that the spin directions are nearly orthogonal relative to the particle momentum in these four bunches. For each bunch, a step function was fit to the vertical polarization as function of time to describe the effect of a resonant spin rotation. An example of such a fit using the rf Wien filter as the spin rotator is shown in Fig. 5. Fig. 6 shows the resulting exclusion regions for the oscillating EDM d_{AC} for the measured frequency range.

The limits of the spin rotation can then be expressed as limits of the coupling of ALPs to the deuteron spin via the oscillating part of the deuteron EDM d_{AC} and/or via the axion wind effect. Since we cannot experimentally distinguish between these two sources, the coupling constants are calculated assuming that either one or the other process produces 100% of the effect. As an example, we show here the limits for the model-independent coupling

[1] Preprint available at https://arxiv.org/abs/2208.07293 .

Preliminary

Figure 7: The 90% upper bound on $|g_{adg}|$ from this experiment (in cyan) is shown along with the bound on $|g_{aNg}|$ from other experiments[3]

of the ALPs to d_{AC}. The Lagrangian is given in terms of the coupling g_{aNg} of the axion to the EDM operator

$$\begin{aligned} L_{aNg} &= \frac{i}{2} g_{aNg}\, a\, \bar{Y}_N \sigma_{\mu\nu} \gamma_5 Y_N F^{\mu\nu} \\ &= \frac{i}{2} \frac{d_{AC}}{a_0}\, a\, \bar{Y}_N \sigma_{\mu\nu} \gamma_5 Y_N F^{\mu\nu}; \end{aligned} \quad (1)$$

where a is the ALP field and $N = n, p$ denotes neutron or proton, respectively. Fig. 7 shows the limit for $|g_{adg}|$ from this experiment in cyan along with bounds for $|g_{aNg}|$ from other experiments (see the publication for details). This experimental study was conducted as a proof-of-principle for searching for axion-like particles in storage rings, with a limited data collection period of four days. However, in future experiments with longer beam times and stronger beam intensities, the sensitivity for detecting these particles can be greatly improved. New types of dedicated storage rings for EDM searches such as proposed by the JEDI Collaboration could also be considered to search for axions in a wider mass range. These would utilize a combination of radial electric and vertical magnetic bending fields. These types of experiments could be further explored at facilities such as RHIC, NICA, or GSI/FAIR, which have or are planning to have polarized hadron beams, and different particles such as protons, deuterons, nuclei, and even leptons could be used to study the effects of spin and isospin on the various couplings. It also offers the opportunity to conduct measurements with different G-factors.

2.2 Electric Dipole Moment (EDM) Searches

Electric Dipole Moments (EDM) of elementary particles are one of the most sensitive tools for the study of physics beyond the Standard Model (BSM), since they break both parity (P) and time-reversal invariance (T) — and, assuming that the CPT theorem holds, also charge parity (CP). The latter is one of the key prerequisites for understanding the apparent asymmetry between matter and antimatter in the universe. Non-zero EDMs exist within the Standard Model, however, these are too small to explain the observed dominance. Therefore, a measurement of EDMs larger than the predictions from the Standard Model would provide a hint towards physics behind the SM and contribute to our understanding of our universe. The goal of the JEDI collaboration with the precursor experiment is a first direct measurement of the deuteron EDM. It is part of a staged approach towards a dedicated high precision, all-electric storage ring for protons[4].
The spin motion in a storage ring can be characterized by the so-called invariant spin axis $\hat{n}$ and the spin tune ν_s. In an ideal storage ring and in the absence of an EDM, the invariant spin axis is vertical. In this case, if one starts with a spin direction within the ring plane, the spin starts precessing about the invariant spin axis and stays in the plane. A non-zero EDM would result in a tilt of the invariant spin axis. In a magnetic ring like COSY the spin tune is given by $\nu_s = G\gamma$, and the tilt of the invariant spin axis caused by an EDM is $\xi = \frac{\eta_{EDM} \beta}{2G}$ in radial direction producing a (small) oscillation of the vertical spin component. In order to generate a net result, additional tools are needed: it has been shown that using an RF Wien filter with the magnetic field axis $\hat{n}_{WF}$ aligned to the invariant spin axis without EDM (i.e. vertical for an ideal ring), the EDM-induced spin rotations can be accumulated when the Wien filter is operated in phase with the spin precession of the stored particles.
This concept has been implemented in two experimental runs at COSY, one in December 2018 and one in February 2021. In order to maintain the resonance condition of the rf Wien filter, a phase-lock feedback had been implemented keeping the relative phase between the Wien filter frequency and the spin precession constant. In addition, the experimental setup allowed intentional variations of $\hat{n}$ in longitudinal direction by means of a solenoidal field (characterized by the angle x^{Sol}) and $\hat{n}_{WF}$ in radial direction by means of a rotation of the Wien filter about its longitudinal axis (characterized by f^{WF}). The resonance strength of Wien filter is then given by

$$\epsilon^2 = \frac{y_0^2}{16\pi^2} \left[f^{WF} - f_0^{WF} \right]^2 + \left[\frac{x^{Sol}}{2\sin(\pi\nu_s)} + x_0^{Sol} \right]^2 \Bigg] .$$

By measuring ϵ as function of f^{WF} and x^{Sol} (called a map) one can determine the setting when the resonance strength of the Wien filter vanishes ($f_0^{WF}; x_0^{Sol}$). This corresponds to the direction of $\hat{n}$. An upper limit of the deuteron EDM can then be extracted by a comparison with simulations assuming $\eta_{EDM} = 0$.
The polarization build-up was measured using two different methods. In Precursor run I, a single bunch was

[3] R. L. Workman et al.: Review of Particle Physics, PTEP, 2022, 083C01 (2022), Figure courtesy of C. O'Hare, https://doi.org/10.5281/zenodo.3932430 .

[4] Abusaif, F. et al.: Storage ring to search for electric dipole moments of charged particles: Feasibility study, https://doi.org/10.23731/CYRM-2021-003

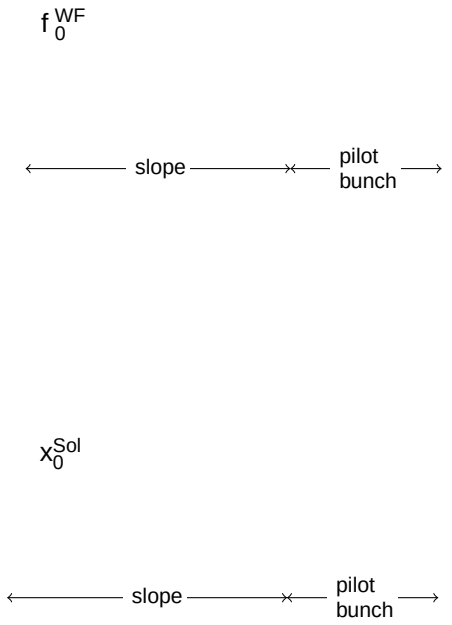

Figure 8: Overview of the current status of all measured maps during Precursor I & II. The upper and lower panel shows the radial and longitudinal component of the invariant spin axis, respectively. The two difference colors for Precursor II Map 1 & 2 represent the two bunches.

used, and the phase-lock feedback as well as the rf Wien filter were acting on the same particles. As the feedback system requires a minimum degree of in-plane polarization to work, the measurement stopped as soon as the out-of-plane spin rotation into the vertical direction was complete. In this setup the slope of the out-of-plane angle $a(n)$ depends on the relative phase f_{rel} between the Wien filter frequency and the spin precession. For Precursor run II, a system of fast switches were implementedat the Wien filter that allowed bunch-selective spin manipulations to be performed (see Sect. 2.3). We then used two bunches in the machine, one for the phase-lock feedback ("pilot bunch") and one for spin rotations by the RF Wien filter. Here, we directly measured the (phase independent) vertical oscillation frequency $f_y = ef_{rev}$. During both runs we measured several maps for systematic studies. We also had several campaigns to mechanically align the COSY components in between the two runs and also calibrated the beam position monitors using beam based alignment.

The results for the directions of n_0^{WF} for various maps are summarized in Fig. 8. There are a number of systematic effects that are currently under investigation.

2.3 Proof of Principle of the Pilot Bunch Technique

There are important spin-physics experiments in storage rings where it is imperative to maintain a large number of spin flips under continuous operation of an rf spin rotator. The pilot bunch approach developed by the JEDI collaboration at COSY (see IKP Annual Report, 2021) uniquely allows either to maintain the exact resonance condition or to fix the detuning of the rf spin rotator with respect to the spin precession frequency by operating in multi-bunch mode, where the spin rotator is gated out (decoupled) from the rf power when a particular (pilot) bunch passes through the spin rotator. The undisturbed (idle) precession of the horizontal polarization of the pilot bunch is continuously monitored using the beam polarimeter. The idle precession frequency is prone to drift, but feedback from the polarimeter is used to correct the spin rotation frequency and maintain either an exact resonance or fixed detuning. The results presented were obtained in 2020 with stored polarized 970 MeV/c deuterons, using the rf Wien filter (WF) employed as a spin rotator.

The case of weak detuning is of interest in its own right, as detuning provides a very interesting insight into the aspects of rf-driven spin rotations in storage rings that have not yet been fully exploited. Here we illustrate the main features of the pilot-bunch technique using the results for vertical polarization obtained in the two-bunch regime. Further details regarding the in-plane polarization and the phase walk are discussed in Vera Shmakova's contribution to this Annual Report (see page 98).

The time structure of the gated rf magnetic field in the WF is shown in Fig. 9. The experiment used of two beam bunches stored simultaneously in COSY, as indicated in Fig. 10. The width of the gate in Fig. 9 is selected according to the bunch length.

Figure 9: The effect of gating on the electromagnetic fields of the rf Wien filter on the signal amplitude.

Polarized beams are stored with vertical initial polarization. The polarizations for the WF-off cycles and those for the pilot-bunch cycles are shown in Fig. 11. In the case of exact resonance, the up-to-down and inverse spin

Figure 10: Pattern of the longitudinal beam intensity pro les of the two deuteron bunches orbiting in the ring.

ips of the active bunch would have been complete and with full amplitude. At nite detuning, the spin ip of the signal bunch would be a partial one with suppressed amplitude and nite offset. The internal polarimeter target only scrapes off the edge (periphery) of the beam that is outside the symmetry center of the polarimeter, which also contributes to the offset of the vertical polarization (see Fig. 11).

The time dependence of the vertical polarization of the pilot and signal bunches, irrespective of a possible detuning, serves as an irrefutable proof of principle for the pilot bunch technique. We t the measured polarization asymmetries to a function $A(t) = a(t - t_0) + b + c\cos(\omega_{SF}(t - t_0) + \phi_{SF})$, where ω_{SF} indicates the spin- ip angular frequency and t_0 denotes the time when the WF was switched on. For the pilot bunch and the cycle with WF switched OFF, the oscillation amplitude is consistent with zero.

2.4 Investigation of Proton Spin Coherence Time

During the last years the JEDI collaboration has performed a sequence of experiments on prolonging and understanding the spin coherence time (SCT) of cooled and bunched deuterons at a beam momentum of $p = 970\,\mathrm{MeV}/c$. It has been shown that sextupole con gurations leading to small chromaticities in the horizontal and vertical plane result in long SCTs in the order of $\tau = 1000\,\mathrm{s}$. The long term strategy for EDM searches aims at an intermediate prototype ring as a demonstrator for key technologies for an electric ring as well as for frozen spin, and has as a nal goal a high precision all-electric storage ring for protons with counter-rotating beams. For such EDM measurements on protons a successful realization of a long spin coherence time is a mandatory requirement.

A rst run on proton SCT was performed at the beginning of 2022. During the experiment a number of challenging observations were made: the distribution of the spin-

Figure 11: Experimental results for one cycle, with two stored bunches in the machine. The red points indicate the vertical polarization when the rf Wien lter (WF) is switched ON (at $t_0 \approx 86\,\mathrm{s}$). The blue points re ect the case for the pilot bunch, i.e., when the rf of the WF is gated out, as indicated in Fig. 9. Black points indicate the situation when, during a different cycle, the WF is completely switched OFF.

Figure 12: Example plot showing the time-evolution of the in-plane polarization of protons after the rotation into the horizontal plane. The vertical line indicates the time when the spin vector reaches the horizontal plane. The spin coherence time is well below 1 s.

resonance frequencies in the beam was too wide to be addressed by an RF solenoid running at xed frequency, the synchrotron side bands (which played no role for deuterons) had a strong in uence on the spin rotation and also other interference terms of unknown origin distorted the pattern of the spin rotation via a Froissart-Stora scan. The best results were achieved when using the RF Wien lter running on a 40 Hz wide frequency band. With this setup some rst data were taken.

Fig. 12 shows an example of the in-plane polarization after rotation in the horizontal plane. The spin coherence time is well below 1 s and, at this stage, it cannot be ex-

cluded, that the slope contains some residual effects from the rotation.
For further planning, additional spin tracking simulations – including the rotation into the horizontal plane – in order to understand the observed features are mandatory. This is a prerequisite for any experimental optimization procedures to come. However, in view of the upcoming cessation of COSY operation by the end of 2023, the JEDI Collaboration has decided to focus on the concluding the precursor studies and not to continue with this topic at COSY.

2.5 Beam and Spin Tracking

Detailed beam and spin dynamics simulations have been performed to explain experimental results with polarized deuterons at COSY and to determine the optimal setting for a long SCT of polarized protons.

Spin tracking simulations in an accurate simulation model of COSY are required to understand the measured data from the precursor experiment with polarized deuterons. The EDM signal results in a tilt of the invariant spin axis from the original vertical direction to the horizontal plane and needs to be distinguished from systematic spin rotations that have the same signature. Therefore, an improved model of COSY was implemented using the Bmad software library. Systematic effects were considered by including magnet displacements, effective dipole shortenings, longitudinal fields, and junction beam deflections. These effects rotate the invariant spin axis in addition to the EDM and need to be analyzed and understood. Recent spin tracking results and methods for determining the invariant spin axis are presented by M. Vitz, page 101. The direct implementation of all measured systematic effects into the simulation model resulted in a tilt of the ISA (Invariant Spin Axis) that was one order of magnitude less than the measured values in the radial and longitudinal directions. As it is very unlikely that this large deviation in the radial direction is due to an EDM, an alternative explanation has to be found. This was recently done by examining the distribution of the ISA under a series of Gaussian distributed quadrupole misalignments. The result of this approach is shown in Fig. 13.
In order to get a complete picture of the ISA distribution under the influence of misalignments, it is necessary to consider the rotations of the quadrupoles as well as other displacements and rotations of the magnets. In Fig. 14 the simulation of an EDM resonance map is shown, taking into account all known and measured systematic effects such as misaligned magnets, multipole fields, etc.
To prepare for SCT optimization for polarized protons at COSY, modeling of the optical setting has been performed. Similar to the optical setting of deuterons, effects influencing the closed orbit, including magnet misalignments and effective dipole lengths, have been implemented in the software library Bmad. The results of the

Preliminary

Figure 13: Distribution of the ISA (radial on the x-axis, long. on the y-axis) by assuming Gaussian distributed quadrupole offsets. A two-dimensional Gaussian fit was applied to the data and is indicated via the grey lines.

Preliminary

Figure 14: The simulated EDM resonance strength is plotted for all known and measured systematic effects versus different Wien filter f_{WF} and solenoidal snake magnet x_{SN} rotation angles. The minimum $f(f_{WF,0}, x_{SN,0})$ indicates the required Wien filter rotation and magnet strength of the snake magnet to align the ISA and EM fields with the corresponding resonance strength $\propto A_{WF} \cdot A_{SN}$ and A_{SN} are the spin rotation angles in the Wien filter respectively in the snake magnet, normalized by 4

experiments conducted in February and March 2022 are compared with a model comprising the real COSY settings for the analysis. Overall, it has been shown that the existing COSY simulation model is capable of describing measurements with protons at COSY by integrating additional systematic effects and implementing a com-

Preliminary

Figure 15: Spin coherence time for a polarized proton beam with optimal sextupole settings. The x-axis is the time and the y-axis is the total polarization.

plex tting algorithm based on the calculation of an orbit response matrix. Additional effects that affect the accuracy of the model include the effective lengths of the quadrupoles, the displacements of the BPMs, the fringe elds, and the effects of the multipole components of the magnets. An improved model with an underlying tting procedure requires additional beam time with protons. Reaching high values of SCT for protons is more challenging compared to deuterons due to a higher anomalous magnetic moment. It has been shown for protons that spin motion is strongly in uenced by nearby intrinsic and integer spin resonances. The strengths of the lattice has been calculated for a typical COSY optical setting and the overall in uence on SCT was predicted. Results for simulations also show that a long SCT with protons cannot be achieved by minimizing the chromaticities alone, as is the case for deuteron beams. The second-order momentum compaction factor must be optimized along with the horizontal and vertical chromaticities. After a 12 million turns spin tracking simulation (see Fig. 15), the total polarization remains above 0.9 (see Guo, page 102).

2.6 Design Study of a Dedicated EDM Ring

Further beam and spin dynamics simulations for a prototype proton EDM ring were carried out to study in detail the advantages and shortcomings of the current lattice. The main problem, which severely limits the optical exibility of the second-order lattice, was found to be the arrangement of the sextupoles, which affects the overall con guration of the lattice. Furthermore, a robust method was developed to optimize the working point of the prototype ring for SCT above 1000 seconds. The established method is also useful to nd the sextupoles settings for long SCT.
Simulations were performed using the Bmad software library to verify the relationship between some important parameters of the optical setting of the lattice and the SCT (see R. Shankar, page 103). Starting from the assumption of a linear system of equations, the optimal arrangement for the three families of sextupoles in an ideal lattice was found by spin-tracking simulations. To optimize the SCT, different values of the second-order optical parameters ξ_x (horizontal chromaticity), ξ_y (vertical chromaticity) and a_1 (second-order momentum compaction factor), which are determined linearly by the eld strengths of the three available sextupole families, were adjusted at xed quadrupole settings.

Preliminary

Preliminary

Figure 16: Evolution of the magnitude of the polarization vector $|\vec{P}(t)|$ of 1000 particles in a Gaussian distributed bunch as a function of the number of simulated turns (upper plot). The decoherence phenomenon is observed as a steady decrease in averaged value of the polarization after several turns. The spin tune spread $D\nu_s(t)$ of the polarization vectors in the particle ensemble from the upper plot is simultaneously determined and plotted against the number of turns (lower plot).

The SCT was determined by tting the steady decrease in the magnitude of the polarization vector $|\vec{P}(t)|$ of the particle ensemble in Fig. 16 (upper plot). The effect of path lengthening, on the other hand, manifests itself as oscillations in the directional shift of the polarization vector, as shown in Fig. 16 (lower plot). Using this analyz-

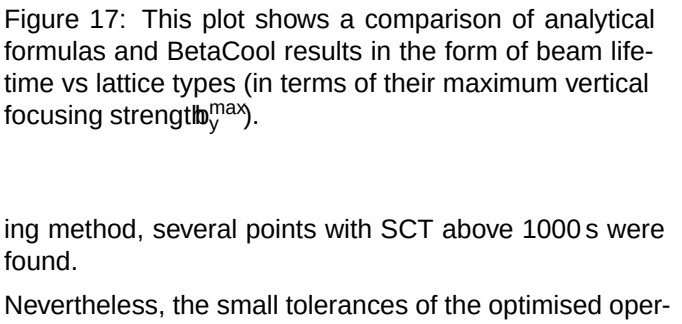

Figure 17: This plot shows a comparison of analytical formulas and BetaCool results in the form of beam lifetime vs lattice types (in terms of their maximum vertical focusing strength b_y^{max}).

ing method, several points with SCT above 1000 s were found.

Nevertheless, the small tolerances of the optimised operating point for meeting the sensitivity criterion are still quite tight and represent a high bar for sextupole precision. While it is envisaged that the lattice improvements investigated so far could relax these tolerances, it is currently unclear whether this will actually be the case. In addition, a deeper look into the mechanisms of decoherence seems to indicate that the spin tune spread varies differently in storage rings with a pure electrostatic bending field compared to those without.

In addition to the SCT, the particle beam in the prototype ring must also provide a sufficiently long beam lifetime. Four different lattices with different maximum focusing strengths, with a maximum Beta function b_y^{max} = 33 m, 100 m, 200 m, 300 m, were generated with the simulation program MADX and studied in the context of beam losses (see S. Siddique, page 104). The aim of these calculations was to find an optimized lattice with minimum systematic effects and maximum beam lifetime. First, four major effects which cause immediate beam loss in a storage ring called Hadronic interactions, Coulomb scatterings, Energy loss straggling, and Touschek effect, were studied and applied analytically. After obtaining results from rough analytical formulae using Wolfram Mathematica, the BetaCool simulation program was used to perform the beam loss calculations. BetaCool is used because it provides a more realistic description of the storage ring. Very good agreement was found between the analytical calculations and the Betacool results, as shown in Fig. 17. As expected, these calculations also show that a lattice with stronger vertical focusing (which means smaller b_y^{max}) provides longer beam lifetimes. Next, a 30 µm diameter carbon pellet was also introduced into the beam to scatter it towards the polarimeter for beam polarization measurements (see S. Siddique, page 104).
These studies have shown that increased beam focusing is beneficial for beam lifetime. In addition, as expected, the beam-target interaction results in significantly higher beam loss rates and a higher beam emittance growth rate. As the beam passes through the target, not all particles experience the same interaction with the target. Due to this inhomogeneous influence of the target on the beam, the beam particles are scattered at different angles and with different momenta. In order to extract the beam at a specific angle, it is necessary to study this interaction in more detail. For this purpose, beam tracking is being performed, including interaction with the target.

2.7 Outlook: Experiments with Polarized Beams and Targets at the GSI/FAIR Storage Rings

A Letter of in Intent (LoI) entitled "Towards experiments with polarized beams and targets at the GSI/FAIR storage rings" has been submitted to the GPAC. The committee encouraged the authors to submit a full proposal. Among the physics topics proposed are axion/ALP searches and the measurement of parity even time reversal odd analyzing power in polarized proton tensor polarized deuteron scattering.
The main goal for 2023 is the preparation of a full proposal for experiments with polarized beams and targets at GSI/FAIR storage rings.

3 Neutrino Physics

The neutrino group is specialized in low-energy neutrino physics with liquid-scintillator (LS) based detectors. Borexino (Sec.3.1), the world's radio-purest 280 ton LS detector in the Laboratori Nazionali del Gran Sasso in Italy took data from May 2007 until October 2021, focused on solar neutrinos, geoneutrinos, and searches for rare processes in coincidence with astrophysical events. JUNO (Sec.3.2) will be the first multi-kton LS detector and it is currently under construction in Jiangmen, China. Its completion is expected by the end of 2023. The success of JUNO strongly depends on the levels of radiopurity that will be achieved. German groups are leading the construction of the 20 ton OSIRIS detector (Sec.3.3), that will monitor the level of radio-purity of the LS during the several months long period of filling the 20 kton JUNO central detector.

3.1 Borexino latest results with solar neutrinos

The Sun is powered via the fusion of hydrogen to helium that can proceed via two distinct mechanisms. The dominant proton-proton (pp) chain is responsible for the production of 99% of the solar energy. The remaining en-

ergy is produced via the sub-dominant carbon-nitrogen-oxygen (CNO) cycle, in which the fusion is catalyzed by the presence of C, N, and O. These two mechanisms are also associated with the emission of electron avor neutrinos (ν_e). These so-called *solar neutrinos* are the only direct messengers about the nuclear reactions occurring in the core of the Sun. In Borexino, the detection of solar neutrinos is primarily based on the scintillation light produced by deposition of energy in scintillating medium by the recoiled electrons from neutrino-electron elastic scattering interaction.

3.1.1 Improved Measurement of CNO-cycle solar neutrinos and its implication for the Standard Solar Model

In 2020, Borexino provided the rst observation of CNO solar neutrinos[5]. This represents the rst experimental evidence of the existence of the CNO cycle in nature. While it is subdominant in the Sun, it is expected to be the dominant stellar hydrogen burning process in the universe. The measurement of CNO solar neutrinos is also relevant for solving one of the key issues of solar physics, the so-called "metallicity-puzzle", where metallicity refers to the abundance of heavy elements in the Sun.

In 2022, Borexino presented an improved measurement of the rate of interaction of CNO solar neutrinos. This measurement was used for the evaluation of the carbon + nitrogen abundance in the solar interior, using solar neutrinos for the rst time. These results were rstly presented at the Neutrino 2022 conference, followed by the publication in Physical Review Letters[6]. This publication was selected by the journal as Editors' Suggestion and was also featured in Physics.

This analysis is based on the data-set collected in the so-called Phase-III period, which extends from January 2017 to October 2021. Several backgrounds contribute in the same energy range as the CNO signal. The latter is represented by a featureless recoiled electron energy spectrum with the end-point energy of 1.517 MeV and with the rate of few counts per day (cpd) in 100 tonnes of LS. Therefore, a multivariate t is performed in order to disentangle the CNO neutrino signal from other solar neutrinos and backgrounds. Similar to the 2020 publication, this t procedure uses constraints on the rates of pep solar neutrinos and the intrinsic ^{210}Bi background to break their spectral degeneracy with the CNO solar neutrinos. In particular, the new ^{210}Bi constraint is now estimated to be (10.8 1.0) cpd/100 t via the counting of decays of its daughter ^{210}Po using pulse shape variable in the cleanest region of the detector, called the Low Polonium Field (LPoF). The LPoF was formed as the result of the detector's thermal stabilisation campaign performed between 2015 and 2016, necessary to minimize the residual convection in the innermost parts of the detector that brought out-of-equilibrium ^{210}Po from peripheral sources to the ducial volume. The updated ^{210}Bi constraint is now lower due to the removal of the 2016 data with high ^{210}Po rate and more precise than the previous value due to the inclusion of new period with stable LPoF after February 2020. After tting, the CNO interaction rate with zero-threshold is estimated to be $6.7^{+2.0}_{0.8}$ cpd/100 tonnes including systematic errors. The observed interaction rate can be converted to a ux of $6.6^{+2.0}_{0.9}$ 10^8cm ^{2}s ^{1} CNO neutrinos at Earth. This result con rms the existence of the CNO cycle at with about 3σ signi cance, which can be interpreted from Fig. 18.

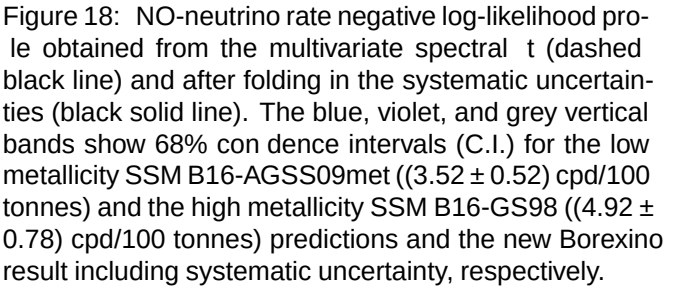

Figure 18: NO-neutrino rate negative log-likelihood pro le obtained from the multivariate spectral t (dashed black line) and after folding in the systematic uncertainties (black solid line). The blue, violet, and grey vertical bands show 68% con dence intervals (C.I.) for the low metallicity SSM B16-AGSS09met ((3.52 ± 0.52) cpd/100 tonnes) and the high metallicity SSM B16-GS98 ((4.92 ± 0.78) cpd/100 tonnes) predictions and the new Borexino result including systematic uncertainty, respectively.

The new result on CNO solar neutrinos is included in a global analysis of all solar neutrino data and KamLAND reactor data in order to investigate the compatibility of experimental measurements with the predictions of the Standard Solar Model (SSM). The resulting solar uxes are found to be in agreement with the high-metallicity SSM (B16-GS98) predictions, while the comparison features a small tension with the low-metallicity SSM (B16-AGSS09met) model. Information on metallicity is also obtained by exploiting the direct dependence of CNO cycle on the C and N abundances in the solar core. The precise measurement of ^{8}B neutrino ux from the global analysis, which strongly depends on temperature, is used "as a thermometer" to decouple the CNO ux dependence on temperature from its dependence on metallicity. This provides the rst-ever measurement of chemical abundances in the Sun's core using solar neutrinos. The C + N abundance with respect to the H in the photosphere is $(5.78^{+1.86}_{1.00})$ 10^{-4}, obtained using extrapo-

[5] Experimental evidence of neutrinos produced in the CNO fusion cycle in the Sun, Nature 587 (2020) 577.

[6] Improved Measurement of Solar Neutrinos from the Carbon-Nitrogen-Oxygen Cycle by Borexino and Its Implications for the Standard Solar Model, Phys. Rev. Lett. 129 (2022) 252701.

Figure 19: Comparison of abundance of (C+ N)/H in the solar photosphere, N_{CN}, from spectroscopy (squares) and using solar neutrinos (circle). The gray area highlights the uncertainty due to the precision of the CNO rate measurement. The white cross marks the result of the very same study repeated changing the reference SSM from the B16-GS98 to the B16-AGSS09met.

Figure 20: Top: Full Borexino rate time series in the RoI dominated by the ^{7}Be solar neutrino signal fitted to the trend model to remove background components. The rate in cpd/100 tonnes is binned in time intervals of 30 days with starting point of the time axis (in days) at 12:00 AM of December 11th 2011, in UTC time. Bottom: Residuals of the time series with respect to the trend model. The blue sinusoidal best fit of the residual rate indicates the presence of a significant annually modulated signal.

lation of the C + N abundance from the core to the photosphere. It was found that the abundance of C and N in the Sun determined with solar neutrinos is in good agreement with all high-metallicity photospheric measurements (MB22, GS98), while it shows 2σ tension with all the low-metallicity photospheric measurements (AGSS09met, C11, AAG21), as demonstrated in Fig. 19.

3.1.2 Search for Low-Energy Signals from Fast Radio Bursts

Fast Radio Bursts (FRBs) are millisecond radio transients observed at the extra-galactic or cosmological distances, with unclear nature of their source. The most popular class of models proposed to explain their origin involve the emission of neutrinos, which could be potentially detected by large Cherenkov or LS detectors. In this analysis, the search for an excess in the number of events produced by neutrino-electron elastic scattering and the inverse beta-decay on protons (IBD) has been performed using the full exposure Borexino data set, between 2007 and 2021. As a result, no statistically significant increase in the number of events over the backgrounds was observed. Furthermore, the strongest upper limits on FRB-associated neutrino fluences of all flavors is obtained in the 0.5–50 MeV neutrino energy range. In 2022, this work was published in European Physical Journal C [7].

3.1.3 Independent determination of the Earth's orbital parameters with solar neutrinos

Borexino collaboration has published the first precise measurement of the Earth's orbital parameters based solely on solar neutrinos in Astroparticle Physics journal [8]. This measurement represents an additional prove of the solar origin of the Borexino signal. The analysis estimates the Earth's orbit eccentricity exploiting the variation of the solar neutrino flux produced in the Sun's core and detected by Borexino on the Earth, caused by the Sun-Earth distance change as a function of time due to the non-circular shape of the orbit. The search for solar neutrino signal modulations in the frequency range between one cycle/year and one cycle/day using the generalized Lomb-Scargle method was performed on the time series of the Borexino measured rate as shown in Fig. 20. The used dataset period ranges from December 11th 2011 to October 3rd 2021. The chosen energy region of interest (RoI) is 300 - 827 keV with a dominant contribution from the mono-energetic ^{7}Be solar neutrinos and a subdominant contribution from pep and CNO neutrinos, including the backgrounds such as ^{210}Bi and ^{85}Kr β decays, γ-ray emitting external backgrounds, and cosmogenic ^{11}C decays. The estimated eccentricity is $e = 0.0184 \pm 0.0032$ (stat+sys). The hypothesis of no annual modulation of the solar neutrino signal due to the eccentricity of Earth's orbit is excluded with a significance greater than 5σ. No other significant modulation frequencies are found. Strong constraints are placed on the amplitudes of other frequencies of interest, such as day-night effects and correlations with the Sun's rotation around its axis. The limits for the percent diurnal modulation and the percent solar rotation day are < 1.3% (90% CL) and 1.8% (90% CL), respectively. These updated bounds are relevant in solar modelling and in constraining various non-standard neutrino interactions.

[7] Search for Low-Energy Signals from Fast Radio Bursts with the Borexino Detector, Eur. Phys. Journal C 82 (2022) 278.

[8] Independent determination of the Earth's orbital parameters with solar neutrinos in Borexino, Astroparticle Physics 145 (2023) 102778.

3.1.4 First directional measurement of sub-MeV solar neutrinos

In 2022, the first measurement of sub-MeV solar neutrinos using their associated subdominant Cherenkov radiation was presented by Borexino. This work was jointly published in Physical Review Letters[9] and Physical Review D[10]. This provided an experimental proof of principle for the exploitation of directional Cherenkov light in future LS-based neutrino experiments using a newly developed technique called Correlated and Integrated Directionality (CID). CID is based on constructing an angular distribution for the solar neutrino events in a energy region of interest (RoI) of 0.54 MeV - 0.74 MeV, dominated by ^{7}Be solar neutrino events. The characteristic angle correlates the direction of first PMT hits of each event (defined between the hit PMT and the reconstructed event vertex) with the known direction from the Sun. The number of solar neutrino events ($N_{solar\ n}$) is then statistically inferred from the contribution of Cherenkov photons correlated to the position of the Sun. The data-set used for the analysis extends from May 2007 to May 2010 referred to as Phase-I period. The extracted number of solar neutrino events in RoI from the best fit of first 2 hits of 19,904 data events is $N_{solar\ n} = 10887^{+2386}_{2103}(stat) \pm 947\ (sys)$. Figure 21 shows the measured angular distribution for the first PMT hits of all selected events along with the best fit. The best fit result is well in agreement with the SSM expectation, rejecting the hypothesis of no neutrino signal at $> 5\sigma$ confidence level. The extracted interaction rate of ^{7}Be solar neutrinos in Borexino is $R_{^{7}Be} = 51.6^{+13.9}_{12.5}$ cpd/100 tonnes by fixing the sub-dominant pep and CNO solar neutrino contributions in RoI to their SSM predictions. It is well in agreement with both SSM predictions as well as Borexino spectral fit results in Phase-I. Furthermore, performing a dedicated calibration of the Cherenkov light is highly recommended for more precise solar neutrino measurements.

An effort is now ongoing to exploit the CID method for the measurement of CNO solar neutrinos using enlarged Borexino dataset. Furthermore, the inferred number of CNO + pep solar neutrinos will be applied as a constraint in the multivariate spectral fit to extract the CNO rate with and eventually even without ^{210}Bi constraint in a combined Phase II + Phase III dataset.

Figure 21: Directional measurement of solar neutrinos by Borexino: The cosα distributions of the first hits of all the selected data events (black points) in RoI compared with the best fit curve (red) for the resulting number of solar neutrinos $N_{solar\ n}$ plus background. All histograms are normalized to the data statistics. It can be seen that the data points cannot be explained by the background-only hypothesis (blue).

3.2 Towards completion of the JUNO detector

The Jiangmen Underground Neutrino Observatory (JUNO) is a multipurpose 20 kton liquid scintillator detector positioned 53 km from the Yangjiang and Taishan nuclear power plants in South China. It is currently under construction in an underground laboratory with a 650 m overburden and with a planned completion in 2023. The experiment is designed for the determination of the neutrino mass ordering, one of the key open questions in neutrino physics. This measurement will be based on the observation of vacuum oscillation pattern of antineutrinos from the two nuclear power plants at 53 km baseline. The unprecedented expected energy resolution of $3\% \sqrt{E[MeV]}$ and the large fiducial volume, offer exciting opportunities for addressing many important topics in neutrino and astro-particle physics. The final design of the detector and the updated JUNO physics strategy are summarized in a recent review paper in Progress in Particle and Nuclear Physics journal[11].

The civil construction of the the JUNO site was completed in December 2021. The Central Detector (CD) will be filled with 20 kton of LS contained in a spherical acrylic vessel with a diameter of 35.4 m. The acrylic panels of the CD detector are being mounted from an installation platform, whose construction was completed in May 2022. The CD is supported by a stainless steel support structure that was finished in June 2022, as it is shown in Fig. 22. On the support structure will be mounted the PMTs with their front-end electronics. The CD will be characterized by high photocathode coverage of 78%, provided by 17,612 20-inch PMTs (LPMTs) and 25,600 3-inch PMTs (SPMTs). The Water Cherenkov Detector (WCD) will consist of 35 kton of ultra-pure water surrounding the CD and will be equipped with 2400 LMPTs. WCD will serve as an active veto of cosmic muons as well as a passive shield against external background. The further key steps towards completion of the JUNO detector are the finalisation of the acrylic vessel construc-

[9] First Directional Measurement of sub-MeV Solar Neutrinos with Borexino, Phys. Rev. Lett. 128 (2022) 091803.

[10] Correlated and Integrated Directionality for sub-MeV solar neutrinos in Borexino, Phys. Rev. D 105 (2022) 052002.

[11] JUNO physics and detector, Progress in Particle and Nuclear Physics, 123 (2022) 103927.

Figure 22: Support structure of the central detector and the installation platform with the workers, photo from June 2022.

tion, PMTs installation, completion of the LS purification plants and OSIRIS pre-detector, and finally 6 months long filling of the LS into CD.

The JUNO LPMTs are of two kinds, about 1/3 is from Hamamatsu and the rest are multi-channel (MCP) PMTs produced by Northern Night Vision Technology (NNVT). All LPMTs have been produced, tested, and instrumented with waterproof potting. An extensive LPMT testing program began in 2017 and elapsed for about four years. A collaboration paper was published in the European Physical Journal C[12] presenting the design of the testing systems and demonstrating a good quality of all accepted PMTs. More than fifteen performance parameters (including the photocathode uniformity) were tested. This constitutes the largest sample of 20-inch PMTs ever produced and studied in detail to date.

The unprecedented size and energy resolution of JUNO enables it to make precise measurement of the oscillated spectrum of reactor antineutrinos, shown in Fig. 23, and to observe the so-called solar and atmospheric oscillation simultaneously. As a result, the measurement of the Δm^2_{31}, Δm^2_{21}, and θ_{12} neutrino oscillation parameters will reach better than sub-percent precision (see Fig. 24). This significant improvement is one of the primary physics goals of the experiment. The new sensitivity estimate for this measurement has been published in a collaboration paper in the Chinese Physics C[13]. These measurements will constitute an important input to other experiments, provide constraints for model building, and enable more precise searches for physics beyond the Standard Model in the neutrino sector.

The damping signatures at reactor spectrum expected in JUNO could be motivated by various new physics models, including quantum decoherence, θ_{13} decay, neutrino absorption, and wave packet decoherence. Their study was published in a collaboration paper in the Journal of

Figure 23: Visible energy spectrum expected in JUNO as measured with the LPMT system with (grey) and without (black) backgrounds.

Figure 24: Relative precision of the neutrino oscillation parameters as a function of JUNO data taking time. The horizontal gray dashed line stands for 1% relative precision. The green dotted and red dotted lines are on top of each other since the statistical-only precision is essentially identical for the Δm^2_{31} and Δm^2_{21} parameters.

High Energy Physics[14]. Here the ability of JUNO to constrain these damping parameters and disentanglement of these different damping signatures have been reported.

Diffuse Supernova Neutrino Background (DSNB) neutrinos represent an integrated neutrino flux from the past supernova explosions in the visible Universe. DSNB has not been detected yet. A comprehensive study on the prospects for its discovery in JUNO was published as a collaboration paper in the Journal of Cosmology and Astroparticle Physics[15]. It reports that even for the pessimistic scenario with non-observation, JUNO would strongly improve the current best limits and exclude a significant region of the model parameter space. Together with the existing water-Cherenkov detector SK-Gd, it stands for the pioneering efforts to first observe the DSNB signal in the next decade. JUNO has a large dis-

[12] Mass Testing and Characterization of 20-inch PMTs for JUNO, Eur. Phys. J. C 82 (2022) 1168.

[13] Sub-percent Precision Measurement of Neutrino Oscillation Parameters with JUNO, Chinese Physics C 46 (2022) 123001.

[14] Damping signatures at JUNO, a medium-baseline reactor neutrino oscillation experiment, J. High En. Phys. 06 (2022) 062.

[15] Prospects for detecting the diffuse supernova neutrino background with JUNO, JCAP10 (2022) 033.

covery potential of S in 3 years of data taking for the nominal theoretical SN models.

JUNO has also potential to search for proton decay in p ! $\bar{\nu}K^+$ mode. The excellent energy resolution of JUNO permits to suppress the sizable background caused by other delayed signals. The sensitivty study was submitted to the Physical Review D as a collaboration paper.[16]

The physics potential of detecting ^{8}B solar neutrinos is exploited at JUNO in a model independent manner by using three distinct channels of the charged-current (CC), neutral-current (NC), and elastic scattering (ES) interactions. Due to the largest-ever mass of ^{13}C nuclei in the liquid-scintillator detectors and the potential low background level, ^{8}B solar neutrinos would be observable in the CC and NC interactions on ^{13}C for the rst time. This has been studied and reported in a collaboration paper submitted to the Astrophysical Journal.[17]

The JUNO sensitivity to ^{7}Be, pep, and CNO solar neutrinos will highly depend on the achieved radio-purity level. Several radio-purity scenarios were considered in a recent study: from the level achieved by the Borexino experiment up to the IBD one (minimum required for the NMO determination), as demonstrated in Fig. 25. For ^{7}Be neutrinos, JUNO can reach the current precision of 2.7% achieved by Borexino after one year of data-taking. For the pep neutrinos, JUNO can improve the current best Borexino result of 17% after two years of data-taking (except for the IBD scenario when 6 years are needed). For the CNO neutrinos, constraint on the rate of pep neutrinos in the spectral t remains crucial and can be achieved using the exiting data and theoretical assumptions. However, JUNO will be able to detect CNO solar neutrinos without the ^{210}Bi constraint applied in the Borexino analysis and to achieve 20% precision in two to four years (except for the IBD scenario). Additionally, JUNO might be able to distinguish the ^{13}N and ^{15}O CNO components for the rst time. The neutrino group has a leading role in this analysis that was presented at the Neutrino 2022 conference. A collaboration paper about these studies is currently under internal review.

Figure 25: Various radiopurity scenarios, considered in the JUNO solar neutrino sensitivity study, compared to the expected spectra of ^{7}Be, pep, ^{13}N, and ^{15}O solar neutrinos for 1 year statistics.

3.3 Online Scintillator Internal Radioactivity Investigation System (OSIRIS) of JUNO

JUNO physics potential strongly depends on the radiopurity levels of the LS that will be achieved. In order to meet the stringent requirements, e.g. U/Th concentration of 10 ^{15} g/g (for the NMO determination) and 10^{17} g/g (for solar neutrino measurement), a scintillator processing system has been built. The LS system includes four puri cation stages (Al_2O_3 column, distillation, water extraction, and steam stripping) as well as storage and mixing tanks. The achieved level of LS radiopurity will be tested in 20 ton detector of OSIRIS (Online Scintillator Internal Radioactivity Investigation System). The OSIRIS design has been optimized to evaluate LS contamination with ^{238}U and ^{232}Th via tagging the ^{214}Bi - ^{214}Po and ^{212}Bi-^{212}Po delayed coincidences occurring in the respective decay chains. After a successful test of each puri cation batch, the LS will be lled into the CD. OSIRIS features an 18 ton LS target within an acrylic vessel of 3 m width and 3 m height. Sixty-four 20-inch Large Photomultiplier tubes (LPMTs) mounted on a stainless steel frame instrument the watershielded target. Twelve additional LPMTs are employed in the water Cherenkov muon veto of OSIRIS, which is seperated from the inner detector by optical foils. The originally foreseen intelligent PMTs (iPMTs), a development of RWTH Aachen that was strongly supported by the neutrino group members, were found to be non-operational after transportation to China. Therefore, the iPMTs were replaced by JUNO LPMTs.

Within OSIRIS, the neutrino group is responsible for the source insertion calibration system, a refurbished Automated Calibration Unit (ACU, see Fig. 26) provided by the Daya Bay collaboration. It features three independent wheels mounted on a turntable, allowing to lower calibration sources directly into the LS volume. In order to maximise the variation of the detector response at different heights, the ACU is placed 1.2 m off-center to the central axis of OSIRIS. Three calibration sources have been purchased by the neutrino group. A multi-gamma source consisting of ^{137}Cs, ^{60}Co, and ^{65}Zn with a combined activity of several kBq will be employed for the calibration of energy and vertex reconstructions. A 435 nm-LED allows the calibration of LPMT timing and charge responses. By tuning its intensity, also higher p.e. occupancies can be investigated. The third source, a low-

[16] JUNO Sensitivity on Proton Decay p ! $\bar{\nu}K^+$ Searches, arXiv:2212.08502v2 (2022), submitted to Physical Review D.

[17] Model Independent Approach of the JUNO ^{8}B Solar Neutrino Program, arXiv:2210.08437 (2022), submitted to APJ.